Received November 29, 2018, accepted January 8, 2019, date of publication January 11, 2019, date of current version February 4, 2019.

Digital Object Identifier 10.1109/ACCESS.2019.2892187

Higher Order Sectorization in FFR-Aided OFDMA Cellular Networks: Spectral- and Energy-Efficiency

JAN GARCÍA-MORALES[1], (Student Member, IEEE), GUILLEM FEMENIAS[2], (Senior Member, IEEE), AND FELIP RIERA-PALOU[2], (Senior Member, IEEE)

[1]UWICORE Laboratory, Universidad Miguel Hernández de Elche, 03202 Elche, Spain
[2]Mobile Communications Group, University of the Balearic Islands, 07122 Palma, Spain

Corresponding author: Guillem Femenias (guillem.femenias@uib.es)

This work was supported in part by the Agencia Estatal de Investigación and Fondo Europeo de Desarrollo Regional (AEI/FEDER, UE), Ministerio de Economía y Competitividad, Spain, through the projects ELISA under Grant TEC2014-59255-C3-2-R and TERESA under Grant TEC2017-90093-C3-3-R.

ABSTRACT It is well known that per macro-site spectral efficiency (SE) can be increased through higher order sectorization (HOS) by radially partitioning the coverage area of each site into multiple sectors and reusing the spectral resources in each sector and across all sites. In order to further reinforce its benefits, HOS can be combined with fractional frequency reuse (FFR) techniques to improve the SE and/or energy efficiency (EE) of the network. This paper presents an analytical framework that is used to assess the sectorization performance in terms of both the SE and EE in the downlink of HOS/FFR-aided orthogonal frequency-division multiple access (OFDMA)-based macro-cellular networks. Tractable mathematical expressions are derived for the round robin, the proportional fair, and the maximum signal-to-interference-plus-noise ratio scheduling rules and the corresponding capacities. The results show the impact of the sectorization gain on the system performance for different cell-edge frequency reuse factor values. Furthermore, an optimization problem for the HOS/FFR-aided OFDMA-based network is addressed, allowing a tradeoff between the EE performance and fairness by suitably dimensioning the FFR inner and outer areas and the corresponding frequency allocation to each of these regions.

INDEX TERMS OFDMA, higher order sectorization, fractional frequency reuse, energy efficiency, optimization.

I. INTRODUCTION

Three-sectorized cell sites have been traditionally used throughout the different generations of cellular radio communications to improve the coverage and spectral efficiency (SE) of these networks in urban and suburban scenarios [1], [2]. The capacity per-site, however, can be increased by using higher-order sectorization (HOS) where, thanks to the use of a large number of antenna panels, the coverage area of a base station (BS) is radially partitioned into multiple horizontal sectors and the spectral resources are reused in different sectors and across cell-sites [3], [4]. Nevertheless, the SE gains provided by the use of HOS come at the cost of an increased cell-site infrastructure, an increased hardware complexity and, specially, an increased energy consumption [5]. In fact, since increasing the number of sectors at a BS site increases the power consumption by a factor proportional to the number of sectors, the energy-efficiency (EE) issue needs to be carefully addressed when considering HOS-aided analytical models [6].

Aside from increasing the overall SE, the provision of a certain degree of quality-of-service (QoS) across the cell, including the data rates provided to mobile stations (MSs) located at the cell edge, is one of the main challenges for network operators of current and future generations of mobile communication systems. In particular, orthogonal frequency division multiple access (OFDMA)-based networks, widely used in modern and envisaged cellular standards [7], suffer from very high levels of intercell interference (ICI) due to

the use of universal frequency reuse plans aiming at overall throughput maximization. In order to tackle this problem while still achieving high levels of SE, multiple ICI coordination (ICIC) strategies have been proposed in the literature (see, for instance, [8] and references therein), among which *static* fractional frequency reuse (FFR), soft frequency reuse (SFR) [9]–[12] and all its variants have been shown to provide a good tradeoff between cell-edge throughput improvement and overall macro-cell SE [13].

Regardless of the particular technology in use, in the downlink of OFDMA-based networks the channel quality varies in time and frequency for different MSs. Such variations in channel conditions can be exploited by using channel-aware schedulers able to allocate each frequency/time resource block (RB) to a MS with favorable channel conditions. Opportunistic maximum signal-to-interference-plus noise ratio (MSINR) scheduling [14] makes the most of the multiuser diversity by allocating the RBs to the MSs experiencing the best channel conditions at the cost of sacrificing fairness. In order to provide a reasonable tradeoff between capacity and fairness, a proportional fair (PF) scheduling rule was first proposed by Kelly *et al.* [15] and then extended by Shakkottai and Stolyar [16]. Using the PF scheduler, the RBs end up being allocated to MSs experiencing the relatively best channel conditions in comparison to their average channel state and thus, the possibility of a MS with a very bad link suffering from long periods of starvation is drastically reduced [17].

The combination of HOS and FFR technologies when using channel-aware scheduling techniques in the downlink of OFDMA-based networks remains largely unexplored, specially when EE issues are taken into consideration, and our main aim in this paper is to make a contribution towards filling in this gap.

A. BACKGROUND WORK

HOS has been extensively covered in the literature (see [3], [18]–[21]). The impact of antenna beamwidth on HOS performance was analyzed in [18]. Even though HOS is much simpler to implement in terms of signal processing, the authors of this work showed that HOS with 12 sectors per site achieves SEs similar to those provided by a conventional three-sectorized system using multiuser MIMO (MU-MIMO). In [3], Joyce *et al.* evaluated the potential coverage and capacity gains of sectorization through extensive simulation and real world trials of HOS deployments (3, 6, 9, 12, and 15 sectors/site) in a 3G/HSPA+ network, showing that remarkable SE gains are possible using HOS configurations well beyond the six sectors per site. The potential performance benefits provided by the use of HOS in millimeter wave (mmWave) networks have been also investigated in [19] and [20] under dense and busy urban scenarios. The results show that higher-order horizontal sectorization in mmWave-based deployments can significantly increase the network capacity. A similar approach was proposed in [21] for ultra-dense cellular networks, also allowing the implementation of virtual sectorization. In this work, a network with two carriers using a layout based on four sectors per carrier was proposed. Unfortunately, aforementioned works [19]–[21] are only based on simulations, do not consider the cost of increasing SE in terms of EE and, furthermore, they only focus on universal frequency reuse schemes that do not consider the use of ICIC techniques, thus largely ignoring the provision of QoS to cell edge MSs.

Recent studies, such as [5] and [22], consider the joint use of HOS and FFR. Specifically, He *et al.* [5], develop a statistical model that, aiming at speeding up network planning and optimization, allows the analytical characterization of the SE performance of HOS deployments in FFR-aided OFDMA-based wireless networks. Al-Falahy and Alani [22], focus on the study of dense mmWave networks using HOS deployments with eight sectors per site and aided by FFR schemes with a frequency reuse factor at the cell edge region equal to the number of sectors per site. This paper shows that FFR can improve the network performance in terms of per user cell-edge data throughput and average cell throughput, and maintain the peak data throughput at a certain threshold. Unfortunately, He *et al.* [5] and Al-Falahy and Alani [22] neglect the important effects of small scale fading, thus precluding the consideration of the use of channel-aware schedulers and, furthermore, they do not take into account the impact of increased power consumption on the EE of FFR-aided HOS deployments.

As one of the main targets of 5G cellular wireless networks is the improvement of EE [23], [24], the performance evaluation of HOS in FFR-aided OFDMA cellular networks should consider both the SE and EE metrics. There are some works in the literature that elaborate on the EE optimization of FFR-aided cellular networks. An optimal power control scheme is derived in [25] allowing a simple energy-efficient optimization problem for FFR-aided OFDMA-based cellular networks. The optimal frequency reuse factor is also obtained when considering the fairness of EE and power consumption. Xie *et al.* [24] jointly analyze the area SE and area EE in a wireless heterogeneous network with inter-tier FFR. Resource allocation based on proportional fairness is used by the authors to balance the SE and user fairness within each cell. FFR and proportional fairness are used to derive the optimal power reduction factor and fractional bandwidth partition that jointly maximize the area SE and area EE. In [26], Altay and Koca present an stochastic geometry-based analysis and optimization of FFR-aided OFDMA-based cellular networks under EE constraints. Unfortunately, none of these research works considers the use of HOS in the respective analytical models. In addition, the average energy consumption of BSs is invariably modeled through a linear function of the average radiated power. These energy consumption models [27] are extremely simplistic and, therefore, it is of paramount importance the formulation of mathematical models that accurately reproduce the actual energy consumption that can be observed in current mobile communications networks [28],

including the possible effects of the joint use of HOS and FFR.

B. CONTRIBUTIONS OF THE PAPER

In this paper we present a novel analytical framework allowing the performance evaluation of HOS and FFR in OFDMA-based multi-cellular networks using channel-aware scheduling rules, while considering a downlink power consumption model specifically refined for HOS/FFR-based systems. The main contributions of this paper can be summarized as follows:

- Extending previous works that solely considered single-antenna configurations (see [13], [17], and references therein), an analytical framework is introduced that allows the performance evaluation, in terms of SE, of HOS/FFR-aided OFDMA-based cellular networks. Towards this end, different sectorization deployments, including the omnidirectional case, the three-sectorized conventional baseline configuration and different HOS-based scenarios are considered in the proposed analytical derivation. Interestingly, tractable mathematical expressions of SE are particularized to resource allocation strategies based on channel-aware schedulers such as the RR, PF or MSINR. It is worth noting that the proposed mathematical model can be straightforwardly adapted to HOS configurations with any number of sectors per site.
- Capitalizing on the derived SE results, and relying on existing power consumption models, analytical expressions are proposed for the characterization of the EE in HOS/FFR-aided OFDMA-based networks. Extensive analytical evaluations and system level simulations are conducted to validate the proposed framework while highlighting the impact of HOS and FFR on the SE and EE of OFDMA-based cellular networks.
- As an exemplary use of the proposed model, and based on the cell-edge frequency reuse factor, the impact of HOS on both the SE and EE performance metrics is analyzed under two FFR arrangements. First, and irrespective of the number of sectors per site, a cell-edge frequency reuse factor equal to 3 is taken under consideration. Second, a cell-edge frequency reuse factor equal to the number of sectors per site is assessed.
- Finally, the tradeoff between the cell-center users' EE performance and the cell-edge users' SE fairness is formulated as an optimization problem whose solution leads to a suitable dimensioning of the FFR inner and outer areas and the corresponding frequency resource allocation to each of these regions. This optimization framework is thoroughly evaluated under different HOS/FFR-based scenarios.

The rest of the paper is organized as follows. In Section II the system model under consideration is introduced alongside with the key assumptions. Section III elaborates on the analytical framework used to derive the average capacity performance of the HOS/FFR-aided OFDMA-based multi-cellular networks. Furthermore, the SE and EE performance metrics are obtained and the sectorization capacity- and the energy-gains are also defined. The EE optimization problem is addressed for HOS/FFR-based deployments in Section IV. Analytical and simulation results are provided in Section V. Finally, the main outcomes of this paper are recapped in Section VI.

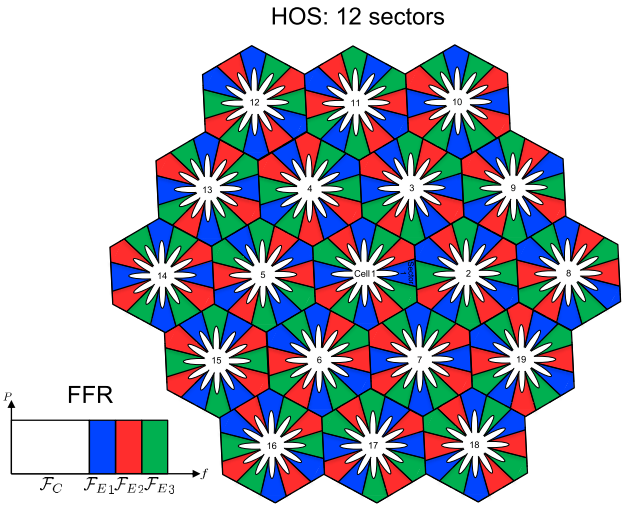

FIGURE 1. Schematic representation of a 12-sector BS deployment using a cell-edge frequency reuse factor equal to 3 (19 BSs).

II. SYSTEM MODEL

Let us consider the downlink of an HOS/FFR-aided OFDMA-based cellular network layout modeled as a regular tessellation of hexagonally-shaped coverage areas, as shown in Fig. 1 for the particular case of a 12-sector per site scenario. The network layout is covered by N_{site} macro-sites, each equipped with one BS located at the center of the hexagonal cell and with N_{sect} sectors per BS. The locations of the MSs at a given time instant are assumed to follow a stationary Poisson point process (PPP) of normalized intensity λ (measured in MSs per area unit). For analytical tractability, the cells are approximated by a circle whose area is the same as the hexagonal one. That is, assuming that the side of the regular hexagon is R_h, the radius of the circular cells is $R = R_h\sqrt{3\sqrt{3}/(2\pi)}$. Without loss of generality, and taking advantage of the symmetry of a regular system, the analysis focuses on the sector 1 of cell 1 (see Fig. 1).

Pilot signals transmitted by the BS are used by the FFR scheme to partition each sector of each cell in the network into both cell-center and cell-edge regions [7], [29]. MSs are classified according to the received pilot's average power level as either center MSs, when it is above a given power threshold P_{th}, or edge MSs, otherwise.

The total system bandwidth is exploited by means of a set $\mathcal{F}_T$ of N_{RB} orthogonal RBs, each consisting of N_{sc} adjacent subcarriers and with a bandwidth B_{RB} small enough to assume that all subcarriers in a subband experience frequency flat fading. The set $\mathcal{F}_T$ is split into a set $\mathcal{F}_C$ of RBs allocated

to the center region and a set $\mathcal{F}_T \backslash \mathcal{F}_C$ of RBs allocated to the edge region. The set $\mathcal{F}_T \backslash \mathcal{F}_C$ is further split into Δ equal subbands, allocating to edge MSs non-overlapping equal-size sets of RBs $\mathcal{F}_{E1}, \mathcal{F}_{E2}, \ldots$ or $\mathcal{F}_{E\Delta}$. The center regions around the BSs are particularly immune to co-channel interference and thus, center MSs in the whole network can share the set $\mathcal{F}_C$ of RBs on a universal frequency reuse basis. The edge regions, however, more prone to intercell interference from neighboring cells, are based on a frequency reuse factor $\Delta \geq 1$. We assume the number of RBs allocated to the center MSs to be $N_C = \rho N_{\mathrm{RB}}$, where ρ is the spectrum allocation factor, while $N_E = (1-\rho)N_{\mathrm{RB}}/\Delta$ represents the number of RBs allocated to the edge MSs. Note that $N_C = N_{\mathrm{RB}} - \Delta N_E$ must be a non-negative integer value less or equal than N_{RB} and thus, $N_E \in \{0, 1, \ldots, \lfloor N_{\mathrm{RB}}/\Delta \rfloor\}$ and ρ can only take values in the set

$$\mathcal{S}_\rho = \left\{ \frac{N_{\mathrm{RB}} - \Delta \lfloor \frac{N_{\mathrm{RB}}}{\Delta} \rfloor}{N_{\mathrm{RB}}}, \frac{N_{\mathrm{RB}} - \Delta(\lfloor \frac{N_{\mathrm{RB}}}{\Delta} \rfloor - 1)}{N_{\mathrm{RB}}}, \ldots, 1 \right\}, \quad (1)$$

where $\lfloor x \rfloor$ denotes the floor operator.

The average received power by MS u, located in an arbitrary sector s served by BS b (where $b \in \{1, \ldots, N_{\mathrm{site}}\}$ and $s \in \{1, \ldots, N_{\mathrm{sect}}\}$) on any subcarrier belonging to the nth RB, can be expressed as

$$P_{b,s,u}(d_u, \theta_u) = P_n L_B(d_{b,u}) G_A(\theta_{b,s,u}), \quad (2)$$

where $P_n = P_T/(N_{\mathrm{sect}} N_{sc} N_{\mathrm{RB}})$, with P_T denoting the maximum available transmit power at the BS (considering uniform power allocation) [30], $L_B(d_{b,u})$ represents the path loss component characterizing the link between sector s of BS b and MS u as

$$L_B\left(d_{b,u}\right) = L_{Bo} - 10\alpha \log_{10}\left(d_{b,u}\right) [\mathrm{dB}], \quad (3)$$

where $d_{b,u}$ is the distance between BS b and the MS u, α is the path loss factor, and L_{Bo} is a reference path loss (measured in dB) when $d_{b,u} = 1$m, $G_A(\theta_{b,s,u})$ represents the antenna gain characterizing the link between sector s and MS u, and it can be calculated as [18]

$$G_A\left(\theta_{b,s,u}\right) = G_{A\max} - \min\left(12\left(\frac{\theta_{b,s,u}}{\theta_{3\mathrm{dB}}}\right)^2, A_{\max}\right) [\mathrm{dB}], \quad (4)$$

where $G_{A\max}$ is the maximum antenna gain, $A_{\max}$ is the maximum attenuation, $\theta_{3\mathrm{dB}}$ represents the 3dB horizontal beamwidth, and $\theta_{b,s,u}$ is the angle between the main radiation direction of sector s and MS u. Note that both $d_{b,u}$ and $\theta_{b,s,u}$ can be written in terms of (d_u, θ_u).

Let us assume that MS u is located in a region S served by the sector 1 (sector of interest) from BS 1 (BS of interest located at the origin of coordinates), where S is a token that represents either the center region C or the edge region E. The instantaneous signal-to-interference-plus-noise ratio (SINR) experienced by this MS on any of the N_{sc} subcarriers conforming the nth RB during an arbitrary scheduling period can be expressed as[1]

$$\gamma_{u,n}^S = \frac{P_{1,1,u}(d_u, \theta_u)|H_{1,1,u,n}|^2}{N_0 \Delta f + I_{u,n}^S(t)}, \quad (5)$$

where $H_{b,s,u,n} \sim \mathcal{CN}(0, 1)$ is the frequency response resulting from the small-scale fading channel linking the sector s and the MS u on the nth RB, N_0 is the noise power spectral density, $\Delta f = B_{\mathrm{RB}}/N_{sc}$ is the subcarrier bandwidth, and $I_{u,n}^S$ denotes the interference term obtained as

$$I_{u,n}^S = \sum_{(b,s)\in\Phi_n^S} P_{b,s,u}(d_u, \theta_u)|H_{b,s,u,n}|^2, \quad (6)$$

where Φ_n^S represents the set of interfering sectors, which is RB-dependent according to which cell region the RB n belongs to. Note that, strictly speaking, $\gamma_{u,n}^S$ and $I_{u,n}^S$ are functions of (d_u, θ_u).

III. SPECTRAL AND ENERGY EFFICIENCY ANALYSIS

A. CELL CAPACITY ANALYSIS

The downlink average cell capacity of the HOS/FFR-aided OFDMA-based cellular network can be expressed as [35]

$$\overline{\eta} = N_{\mathrm{sect}} \overline{\eta}_{\mathrm{sect}} = N_{\mathrm{sect}} \sum_{k=1}^{\infty} Pr\{M_{\mathrm{sect}} = k\} \overline{\eta}_{\mathrm{sect}}(k), \quad (7)$$

where $\overline{\eta}_{\mathrm{sect}}$ is the downlink average capacity per sector, $Pr\{M_{\mathrm{sect}} = k\}$ is used to denote the probability that there are exactly $M_{\mathrm{sect}} = k$ MSs in a given sector, and $\overline{\eta}_{\mathrm{sect}}(k)$ is the downlink average capacity of a sector populated by k MSs. As the MSs are independently and uniformly distributed over the service coverage area with a density of λ MSs per area unit, the probability distribution of the number of MSs falling within a sector of area $A_r^{1,1}$ (the sector of interest) follows a Poisson distribution, thus implying that

$$Pr\{M_{\mathrm{sect}} = k\} = \frac{(\lambda A_r^{1,1})^k e^{-\lambda A_r^{1,1}}}{k!}. \quad (8)$$

Furthermore, as the sector of interest is split into a center region and an edge region, out of the k MSs located in this sector, there will be k_C MSs located in the center region and $k - k_C$ MSs located in the edge region. Hence, denoting by P_r^C the probability that a MS is located in the center region, the downlink average capacity provided by a sector populated by k MSs can be obtained as

$$\overline{\eta}_{\mathrm{sect}}(k) = \sum_{k_C=0}^{k} \binom{k}{k_C} \left(P_r^C\right)^{k_C} \left(1 - P_r^C\right)^{k-k_C} \times \left[N_C \overline{\eta}_n^C(k_C) + N_E \overline{\eta}_n^E(k - k_C)\right], \quad (9)$$

[1] As it is typically done in the background literature (see [12], [31]–[33]), and for analytical simplicity, only pathloss and small scale fading are taken into account in this paper. In future research, the current framework will be extended to take into account the large scale fading (shadowing) and irregular BS deployments as well [34].

where $\overline{\eta}_n^S(k)$ is the average capacity on the nth RB when there are k MSs in region S.

The probability that an arbitrary MS in sector 1 of BS 1 is located in the center region or edge region can be derived as

$$P_r^C = \mathbb{P}\left\{P_{th} \leq P_{1,1,u}(d_u, \theta_u) \leq \infty\right\} = \int_{-\frac{\pi}{N_{\text{sect}}}}^{\frac{\pi}{N_{\text{sect}}}} \int_{R_0}^{R_{th}(P_{th},\theta)} f_{d_u}(d) f_{\theta_u}(\theta)\, \mathrm{d}d\, \mathrm{d}\theta, \quad (10)$$

and

$$P_r^E = \mathbb{P}\left\{0 \leq P_{1,1,u}(d_u, \theta_u) \leq P_{th}\right\} = 1 - P_r^C, \quad (11)$$

respectively, where, relying on the uniform distribution of MSs, the probability density functions (PDFs) of random variables d_u and θ_u can be correspondingly expressed as

$$f_{d_u}(d) = \frac{2d}{R^2 - R_0^2}, \quad R_0 \leq d \leq R, \quad (12)$$

and

$$f_{\theta_u}(\theta) = \frac{N_{\text{sect}}}{2\pi}, \quad -\frac{\pi}{N_{\text{sect}}} \leq \theta \leq \frac{\pi}{N_{\text{sect}}}, \quad (13)$$

and the limit of integration $R_{th}(P_{th}, \theta_u)$ can be defined, by combining (2) and (3), as

$$R_{th}(P_{th}, \theta_u) = \min\left(\max\left(\left(\frac{P_{th}}{P_n G_A(\theta_u) L_{Bo}}\right)^{-1/\alpha}, R_0\right), R\right). \quad (14)$$

The average sector capacity on the nth RB allocated to region S in sector 1 of BS 1 when there are $M_S = k$ MSs, can be obtained as

$$\overline{\eta}_n^S(k) = \mathbb{E}_{\gamma_n^A|M_S}\left\{B_{\text{RB}} \log_2(1 + \gamma_n^S)|M_S = k\right\} = B_{\text{RB}} \log_2 e \int_0^\infty \frac{1 - F_{\gamma_n^S|M_S}(x|k)}{1 + x}\, \mathrm{d}x, \quad (15)$$

where γ_n^S denotes the instantaneous SINR experienced on the nth RB of region S and $F_{\gamma_n^S|M_S}(x|k)$ is its cumulative distribution function (CDF).

In order to obtain mathematically tractable average capacity expressions, the CDF $F_{\gamma_n^S|M_S}(x|k)$ has to be calculated for the specific scheduling policy applied by the resource allocation algorithm. In the following subsections this CDF will be obtained for the PF scheduling rule and then it will be particularized to both the MSINR and the RR schedulers.

1) PF SCHEDULING

The PF scheduler, exploiting the knowledge of the instantaneous SINRs experienced by all MSs $q \in \mathcal{M}_S$, allocates RB $n \in \mathcal{F}_S$ to the MS $u \in \mathcal{M}_S$ satisfying

$$u = \arg \max_{q \in \mathcal{M}_S} \{w_q(t) \gamma_{q,n}(t)\}, \quad (16)$$

where $\mathcal{M}_S$ is the set indexing all MSs in region S, and $w_q(t) = 1/\mu_q(t)$ is the weighting (prioritization) coefficient for MS q that, in this case, depends on the short-term averaged evolution of channel-state information that is obtained using a moving average over a window of W scheduling periods as [35]

$$\mu_q(t) = \left(1 - \frac{1}{W}\right) \mu_q(t-1) + \sum_{n \in \mathcal{F}_S} \iota_{q,n}(t) \frac{\gamma_{q,n}(t)}{W}, \quad (17)$$

with $\iota_{q,n}(t)$ denoting the indicator function of the event that MS q is scheduled on RB n during scheduling period t.

Using this definition, and taking into account that, given the positions of MSs in region S, it is assumed that on each RB n in region S the MSs are statistically equivalent in terms of the scheduling metrics, the conditional CDF $F_{\gamma_n^S|M_S}(x|k)$ in (15) can be obtained as [35]

$$F_{\gamma_n^S|M_S}^{\text{PF}}(x|k) = \int_{-\frac{\pi}{N_{\text{sect}}}}^{\frac{\pi}{N_{\text{sect}}}} \int_{R_L^S}^{R_U^S} \left(F_{\gamma_{u,n}^S|d_u,\theta_u}(x|d,\theta)\right)^k \frac{f_{d_u}(d) f_{\theta_u}(\theta)}{P_r^S}\, \mathrm{d}d\, \mathrm{d}\theta, \quad (18)$$

where $R_L^C = R_0$, $R_U^C = R_{th}(P_{th}, \theta)$, $R_L^E = R_{th}(P_{th}, \theta)$, $R_U^E = R$, and the conditional CDF $F_{\gamma_{u,n}^S|d_u,\theta_u}(x|d,\theta)$ of the instantaneous SINR $\gamma_{u,n}^S$ experienced by MS u located in region S can be calculated as in [11]

$$F_{\gamma_{u,n}^S|d_u,\theta_u}(x|d,\theta) \triangleq \mathbb{P}\{\gamma_{u,n}^S \leq x|d_u, \theta_u\} = 1 - e^{-\frac{xN_0\Delta f}{\bar{\gamma}_0}} \prod_{(b,s)\in\Phi_n^S} \frac{1}{1 + \frac{x\bar{\gamma}_{b,s}}{\bar{\gamma}_0}}, \quad (19)$$

where $\overline{\gamma}_0 = P_{1,1,u}(d_u, \theta_u)$ represents the average received signal power and $\overline{\gamma}_{b,s} = P_{b,s,u}(d_u, \theta_u)$ is the average interfering signal power from interfering sector $A_{b,s}$.

2) MSINR SCHEDULING

When implementing the MSINR scheduling rule, in each scheduling period and on each RB n in region S, the BS serves the MS experiencing the highest instantaneous SINR, that is,

$$\gamma_n^S = \max_{q \in \mathcal{M}_S} \left\{\gamma_{q,n}(t)\right\}. \quad (20)$$

Note that the MSINR scheduling rule is equivalent to the PF scheduler specified in (16) by setting the weighting coefficients to $w_q(t) = 1\ \forall\ q \in \mathcal{M}_S$. In this case, following a reasoning similar to that used to analyses the PF scheduling rule, the conditional CDF of γ_n^S, conditioned on the event that there are $M_S = k$ MSs in region S and on the set $(\boldsymbol{d}, \boldsymbol{\theta}) = \{(d_u, \theta_u)\}_{\forall u \in \mathcal{M}_S}$, can be expressed as

$$F_{\gamma_n^S|M_S,\boldsymbol{d},\boldsymbol{\theta}}(x|k, \boldsymbol{d}, \boldsymbol{\theta}) = \prod_{u \in \mathcal{M}_S} F_{\gamma_{u,n}^S|d_u,\theta_u}(x|d,\theta). \quad (21)$$

Consequently, as on each RB n in region S the MSs are statistically equivalent in terms of SINR after averaging over (d_u, θ_u), the conditional CDF $F_{\gamma_n^S|M_S}(x|k)$ in (15) simplifies to

$$F_{\gamma_n^S|M_S}^{\text{MSINR}}(x|k) = \left[\int_{-\frac{\pi}{N_{\text{sect}}}}^{\frac{\pi}{N_{\text{sect}}}} \int_{R_L^S}^{R_U^S} F_{\gamma_{u,n}^S|d_u,\theta_u}(x|d,\theta) \times \frac{f_{d_u}(d) f_{\theta_u}(\theta)}{P_r^S}\, \mathrm{d}d\, \mathrm{d}\theta\right]^k. \quad (22)$$

3) RR SCHEDULING

A RR scheduler allocates RBs to MSs in a fair time-sharing approach. Since the SINRs experienced by MSs in region S on each RB n are statistically equivalent, serving $M_S = k$ MSs using a RR scheduling policy is equivalent to serving $M_S = 1$ MSs with MSINR or PF (even when MSs are selected with non uniform probability). Therefore, the conditional CDF $F_{\gamma_n^S|M_S}(x|k)$ in (15) simplifies to

$$\begin{aligned} &F^{\mathrm{RR}}_{\gamma_n^S|M_S}(x|k) \\ &= F^{\mathrm{MSINR}}_{\gamma_n^S|M_S}(x|1) = F^{\mathrm{PF}}_{\gamma_n^S|M_S}(x|1) \\ &= \int_{-\frac{\pi}{N_{\mathrm{sect}}}}^{\frac{\pi}{N_{\mathrm{sect}}}} \int_{R_L^S}^{R_U^S} F_{\gamma^S_{u,n}|d_u,\theta_u}(x|d,\theta)\, \frac{f_{d_u}(d) f_{\theta_u}(\theta)}{P_r^S}\, \mathrm{d}d\, \mathrm{d}\theta. \end{aligned} \quad (23)$$

B. SPECTRAL-EFFICIENCY AND SECTORIZATION CAPACITY-GAIN

The average cell spectral-efficiency $\overline{\tau}$ is defined as the average cell capacity per Hz (measured in bps/Hz). In order to stress its dependency with respect to the FFR parameters P_{th} and ρ, the average cell spectral-efficiency can be expressed as

$$\overline{\tau}(P_{th}, \rho) \triangleq \frac{\overline{\eta}(P_{th}, \rho)}{B_{\mathrm{RB}} N_{\mathrm{RB}}} = \frac{\rho \overline{\eta}^C(P_{th}) + \frac{(1-\rho)}{\Delta} \overline{\eta}^E(P_{th})}{B_{\mathrm{RB}}}, \quad (24)$$

where $\overline{\eta}^C(P_{th})$ and $\overline{\eta}^E(P_{th})$ are the average cell-center and -edge capacities per RB (measured in bps/RB), respectively.

Additionally, the sectorization capacity-gain $G_{\overline{\eta}}$ can be expressed as [6]

$$G_{\overline{\eta}} \triangleq \frac{\overline{\eta}^{\,\mathrm{sect}_{N_{\mathrm{sect}}}}}{\overline{\eta}^{\,\mathrm{omni}}}, \quad (25)$$

where $\overline{\eta}^{\,\mathrm{sect}_{N_{\mathrm{sect}}}}$ represents the average cell capacity $\overline{\eta}$ of a sectorized network with N_{sect} sectors, and $\overline{\eta}^{\,\mathrm{omni}}$ is the average cell capacity $\overline{\eta}$ obtained when using an omnidirectional antenna.

C. ENERGY-EFFICIENCY AND SECTORIZATION ENERGY-GAIN

The average cell energy-efficiency $\overline{\kappa}$ (measured in bps/Watt) is defined as the expected cell throughput divided by the total BS power consumption. Then, the average cell EE can be expressed as

$$\overline{\kappa}(P_{th}, \rho) \triangleq \frac{\overline{\eta}(P_{th}, \rho)}{P_{\mathrm{av}}(P_{th}, \rho)}, \quad (26)$$

where $\overline{\eta}(P_{th}, \rho)$ is given by the numerator in (25) and $P_{\mathrm{av}}(P_{th}, \rho)$ is the average power consumption per site, to be analyzed next in detail and that, as its notation reveals, depends on the FFR parameters P_{th} and ρ.

The proposed downlink power consumption model builds on previous results given in [6], [27], [28], [36], and [37], but taking into account the specific features of HOS/FFR-based systems, which results in an average consumed power

$$\begin{aligned} P_{\mathrm{av}}(P_{th}, \rho) = {} & P_{\mathrm{ps}}(P_{th}, \rho) + P_{\mathrm{bh}}(\overline{\eta}(P_{th}, \rho)) \\ & + P_{\mathrm{bb}}(\overline{\eta}(P_{th}, \rho)) + P_{\mathrm{tr}}(\rho) + P_{\mathrm{pa}}(\rho), \end{aligned} \quad (27)$$

where $P_{\mathrm{ps}}(P_{th}, \rho)$ represents the power supply consumption for the different modules of the BS and depends on the specific FFR settings [36], $P_{\mathrm{bh}}(\overline{\eta}(P_{th}, \rho))$ and $P_{\mathrm{bb}}(\overline{\eta}(P_{th}, \rho))$ denote the backhaul power consumption and the baseband signal processing power consumption, respectively, with both quantities, as shown in [28] and [37], being dependent on the average cell capacity $\overline{\eta}(P_{th}, \rho)$ (see (25)), thus making them directly dependent on the FFR parameters. Finally, the RF transceiver power consumption $P_{\mathrm{tr}}(\rho)$ and the consumed power by the power amplifier $P_{\mathrm{pa}}(\rho)$ are only related to the spectrum allocation factor ρ [6], [36]. In order to gain further insight regarding the effects the FFR parameters exert of the average power consumption, each term is now carefully examined.

Typically, the efficiency of the DC power supply module is around 85% to 90% [36]. Hence, the supply power consumption can be calculated as

$$\begin{aligned} P_{\mathrm{ps}}(P_{th}, \rho) = \zeta_{\mathrm{ps}} \big[& P_{\mathrm{bh}}(\overline{\eta}(P_{th}, \rho)) + P_{\mathrm{bb}}(\overline{\eta}(P_{th}, \rho)) \\ & + P_{\mathrm{tr}}(\rho) + P_{\mathrm{pa}}(\rho) \big], \end{aligned} \quad (28)$$

where ζ_{ps} is the power supply coefficient defined as the ratio between the power loss due to power supply and the power required for other modules in the BS. The value of ζ_{ps} is around 0.1 to 0.15 [36].

The backhaul is used to transfer data between the BS and the core network. According to [37], the backhaul power consumption is commonly modeled as the sum of two parts, a data-traffic-independent one and a data-traffic-dependent one, with the later one being proportional to the average cell capacity. Hence, the backhaul power consumption can be expressed as

$$P_{\mathrm{bh}}(\overline{\eta}(P_{th}, \rho)) = P_{\mathrm{bho}} + \overline{\eta}(P_{th}, \rho) P_{\mathrm{bht}}, \quad (29)$$

where P_{bho} is the backhaul fixed power consumption (data-traffic-independent power) that typically depends on the distances between the BS and the core network and the system topology, and P_{bht} represents the traffic-dependent backhaul power consumption coefficient (in Watt/bps) [37].

The power consumption of different baseband signal processing functions (such as scrambling, CRC Check, encoding, bit interleaving, modulation, or IFFT) increases by a factor of N_{sect} [36]. Furthermore, as stated by Björnson *et al.* [28], the power consumption accounting for channel coding and modulation is proportional to the throughput (measured in bps). Therefore, the baseband signal processing power consumption can be quantified as

$$P_{\mathrm{bb}}(\overline{\eta}(P_{th}, \rho)) = N_{\mathrm{sect}} \left(P_{\mathrm{bbo}} + \frac{\overline{\eta}(P_{th}, \rho)}{N_{\mathrm{sect}}} P_{\mathrm{bbt}} \right), \quad (30)$$

where P_{bbo} is the fixed power consumption of different functions in baseband, and P_{bbt} represents the traffic-dependent power-coefficient required for coding and modulation (in Watt/bps) [28].

The RF transceiver power consumption, as described in [28] and [36], includes the power required to run the

circuit components (such as converters, mixers, and filters) and the power consumed by the local oscillator. Furthermore, as stated in [6], RF transceiver power and PA power consumptions are proportional to the RF resources assigned (i.e., the number of assigned RBs) and the number of sectors/BS, that is,

$$P_{\text{tr}}(\rho) = a(\rho) N_{\text{sect}} P_{\text{trs}}, \tag{31}$$

where P_{trs} is the per-sector power consumed by circuit components and the local oscillator when all RF resources are assigned, and $a(\rho)$ represents the normalized resource utilization coefficient per sector that can be obtained as[2]

$$a(\rho) \triangleq \frac{N_C + N_E}{N_{\text{RB}}} = \rho + \frac{(1-\rho)}{\Delta}. \tag{32}$$

The power consumed by the PA is proportional to the radiated transmit power and is affected by the cable and coupling losses as

$$P_{\text{pa}}(\rho) = a(\rho) N_{\text{sect}} \left(\frac{P_{\text{tx}}}{\varepsilon_{\text{pae}} \sigma_{\text{feed}}} \right), \tag{33}$$

where P_{tx} is the maximum radiated transmit power per sector, ε_{pae} is the power amplifier efficiency and σ_{feed} represents the feeder cable losses. Since $P_{\text{tx}} = P_T / N_{\text{sect}}$, the PA power consumption does not depend on the number of sectors [36], hence it can be rewritten, using also (32), as

$$P_{\text{pa}}(\rho) = a(\rho) \frac{P_T}{\varepsilon_{\text{pae}} \sigma_{\text{feed}}} = \frac{\rho P_T + \frac{(1-\rho)}{\Delta} P_T}{\varepsilon_{\text{pae}} \sigma_{\text{feed}}}. \tag{34}$$

The sectorization energy-gain $G_{\overline{\kappa}}$ of different sectorization orders (taking as baseline the omnidirectional case), in this paper, is defined as

$$G_{\overline{\kappa}} \triangleq \frac{\overline{\kappa}^{\,\text{sect}_{N_{\text{sect}}}}}{\overline{\kappa}^{\,\text{omni}}}, \tag{35}$$

where $\overline{\kappa}^{\,\text{sect}_{N_{\text{sect}}}}$ represents the average cell energy-efficiency of a sectorized network with N_{sect} sectors, and $\overline{\kappa}^{\,\text{omni}}$ is the omnidirectional case average cell energy-efficiency.

IV. EE OPTIMIZATION

One of the major issues when dealing with FFR-based strategies is the optimization of throughput-related utility functions with constraints on the degree of fairness among users arbitrarily located throughout the cell. In this section we focus on optimization of the FFR parameters aiming at maximizing the average cell EE under HOS, subject to certain constraints of the performance of the edge users.

While the general scope of the earlier works on EE optimization was to minimize the power consumption with constraints on the minimum average cell capacity [38], FFR parameter optimization problems aim at maximizing EE with constraints on the minimum average capacity provided to the cell-edge users [25] (see also [26]). Based on the foregoing research works, we apply here the optimal QoS-constrained design (QoScD) where the FFR-related parameters are selected to warrant a prescribed trade-off between the average capacity provided to cell-center MSs and that provided to MSs located in the cell-edge. Note that we introduced a similar design in [17] for FFR, later extended to SFR scheme in [39], but targeting the SE and disregarding the use of sectorization. Using a QoScD-based FFR design, both a minimum average cell capacity and per-region capacity constraints are simultaneously guaranteed.

The QoScD approach aims at determining both the set of power thresholds and the spectrum allocation factor that maximize the average cell energy-efficiency $\overline{\kappa}$ under the constraint that the cell-edge user's spectral efficiency is at least equal to a fixed fraction q of the one provided to the cell-center MSs. Hence, the constrained optimization problem can be formulated in terms of the QoS factor q as

$$\begin{aligned} &\left(P_{th}^*, \rho^*\right) \\ &\quad = \arg \max_{\substack{0 \le P_{th} \le \infty \\ \rho \in \mathcal{S}_\rho}} \overline{\kappa}(P_{th}, \rho), \\ &\qquad \text{subject to } \frac{1-\rho}{\Delta} N_{\text{RB}} \overline{\eta}^E(P_{th}) \ge q\, \rho N_{\text{RB}} \overline{\eta}^C(P_{th}). \end{aligned} \tag{36}$$

By transforming the previous constraint we can obtain an expression of ρ as a function of P_{th} as

$$\rho(P_{th}) \le \left(1 + \Delta q \frac{\overline{\eta}^C(P_{th})}{\overline{\eta}^E(P_{th})} \right)^{-1}, \quad 0 \le P_{th} \le \infty, \tag{37}$$

Note that this expression already provides some insight regarding the FFR parameters and the SE and EE performance. In particular, the maximum possible value of $\rho(P_{th})$ for a given Δ, decreases when the quality factor q increases, that is, enforcing a higher degree of fairness among the cell-center and the cell-edge spectral efficiencies results in a smaller value of ρ, thus indicating that more spectrum is allocated to the cell-edge. Also, setting the quality factor to

$$q = \frac{\overline{\eta}^E(P_{th})}{\Delta \overline{\eta}^C(P_{th})},$$

the maximum $\rho(P_{th})$ becomes $\rho_0 = 0.5$, with ρ_0 representing the fixed spectrum allocation factor often used in Fixed-spectrum-allocation designs (FxD) [17], [33]. Similarly, setting

$$q = \frac{A_r^{1,1,E} \overline{\eta}^E(P_{th})}{\Delta A_r^{1,1,C} \overline{\eta}^C(P_{th})}$$

with $A_r^{1,1,E}$ and $A_r^{1,1,C}$ representing the edge and central areas, respectively, for the BS/sector of interest, the maximum spectrum allocation becomes $\rho_0 = A_r^{1,1,E} / A_r^{1,1,C}$, thus leading to the so-called Area-proportional design (ApD) [10], [32]. In light of these remarks, it is worth noting that the proposed QoScD design can be transformed into the classical FxD and ApD strategies by a suitable choice of q. As stated in [32],

[2]When a is equal to unity, all the RF resources are assigned during the observation time [6].

TABLE 1. Network parameters.

System parameter	Value
Carrier frequency (GHz)	2
Total bandwidth (MHz)	20
Number of sites N_{site}	19
Number of sectors per site N_{sect}	1/3/6/12
Cell radius R (m)	500
Minimum distance R_0 (m)	35
Power spectral density of noise (dBm/Hz)	-174
Bandwidth per RB B_{RB} (kHz)	180
Subcarrier spacing Δf (kHz)	15
Number of resource blocks N_{RB}	100
Subcarriers per RB N_{sc}	12
Maximum BS transmit power P_T (Watt)	40
Power supply coefficient ζ_{ps}	0.1
Backhaul fixed power P_{bho} (Watt)	0.825
Backhaul coefficient P_{bht} (Watt/Gbps)	0.25
Baseband fixed power P_{bbo} (Watt)	0.15167
Baseband coefficient P_{bbt} (Watt/Gbps)	0.1
Transceiver per-sector power P_{trs}(Watt)	3
Power amplifier efficiency ε_{pae}	0.39
Feeder cable losses σ_{feed}	0.4989
Omnidirectional antenna gain $G_{A^{\text{omni}}}$ (dBi)	14
Maximum antenna gain $G_{A\text{max}}$ (dBi)	15.5/19.8/22 (3/6/12)
Antenna maximum attenuation A_{max} (dB)	20/23/26 (3/6/12)
Horizontal beamwidth $\theta_{3\text{dB}}$ (Degrees)	70/35/17.5 (3/6/12)
Small-scale fading model	Rayleigh channel
Path loss model $L_B(d)$ (dB)	$15.3 + 37.6 \log_{10}(d)$
Monte-Carlo trials	1,000

the optimal ρ is located at the extremal points of inequality (37). Hence, we may define $\rho^{\dagger}(P_{th})$ as

$$\rho^{\dagger}(P_{th}) \triangleq \max_{\rho \in \mathcal{S}_{\rho}} \rho(P_{th}), \quad 0 \leq P_{th} \leq \infty, \tag{38}$$

where the superscript $(\cdot)^{\dagger}$ is used to indicate the maximum value of ρ in the set $\mathcal{S}_{\rho}$ that, for each value of P_{th}, fulfills the inequality in (37). Then, the optimization problem (36) can be rewritten as

$$P_{th}^{*} = \arg \max_{0 \leq P_{th} \leq \infty} \overline{\kappa} \left(P_{th}, \rho^{\dagger}(P_{th}) \right), \tag{39}$$

and

$$\rho^{*} = \rho^{\dagger}(P_{th}^{*}). \tag{40}$$

Problem (39) can be solved by using standard software optimization packages (e.g., Matlab), while (40) leads to a simple substitution.

V. PERFORMANCE EVALUATION

In order to validate the proposed framework, a 19-cell HOS/FFR-aided OFDMA-based network is considered under different sectorization deployments. As stated in previous sections, MSs are distributed over the coverage area using a PPP of intensity λ. The main system parameters used in this study are summarized in Table 1. The power consumption model parameters are obtained from a variety of prior works: power supply efficiency is set according to [36], backhaul-related power and coefficient have been obtained from [37],

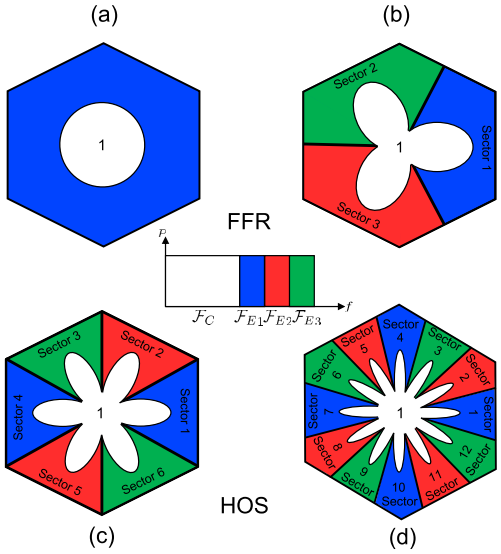

FIGURE 2. Schematic representation of different sectorial deployment layouts using $\Delta = 3$. (a) Omnidirectional. (b) 3 sectors. (c) 6 sectors. (d) 12 sectors.

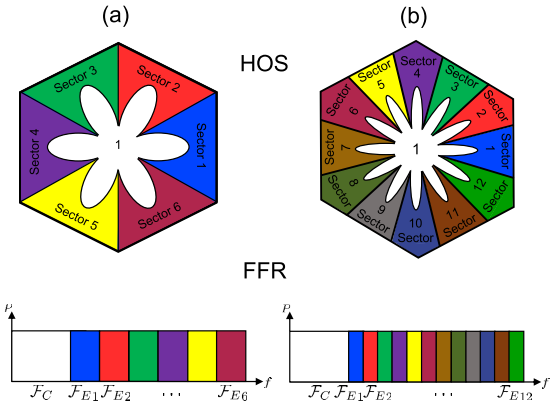

FIGURE 3. Schematic representation of different sectorial deployment layouts using $\Delta = N_{\text{sect}}$. (a) 6 sectors. (b) 12 sectors.

baseband and transceiver power consumption parameters and PA efficiency have been set according to [28] and [36], and feeder cable losses according to [6]. The radio access network parameters and propagation models are based on [40].

A. HOS/FFR COMPARISON

In this subsection, HOS/FFR deployments are evaluated and compared using analytical results and system level simulations under RR, PF and MSINR scheduling policies. As shown in Fig. 2, the analysis concentrates on the omnidirectional case (Fig. 2a), the 3-sector BS (Fig. 2b), the 6-sector BS (Fig. 2c) and the 12-sector BS (Fig. 2d) configurations (i.e., $N_{\text{sect}} \in \{1, 3, 6, 12\}$). In HOS-based configurations (see Figs. 2c and 2d), the main directions of the sector antennas are offset with respect to the 3-sector layout to avoid neighboring sectors pointing at each other when using $\Delta = 3$ [5]. Alternatively, another FFR arrangement based on the cell-edge frequency reuse factor $\Delta = N_{\text{sect}}$ is studied

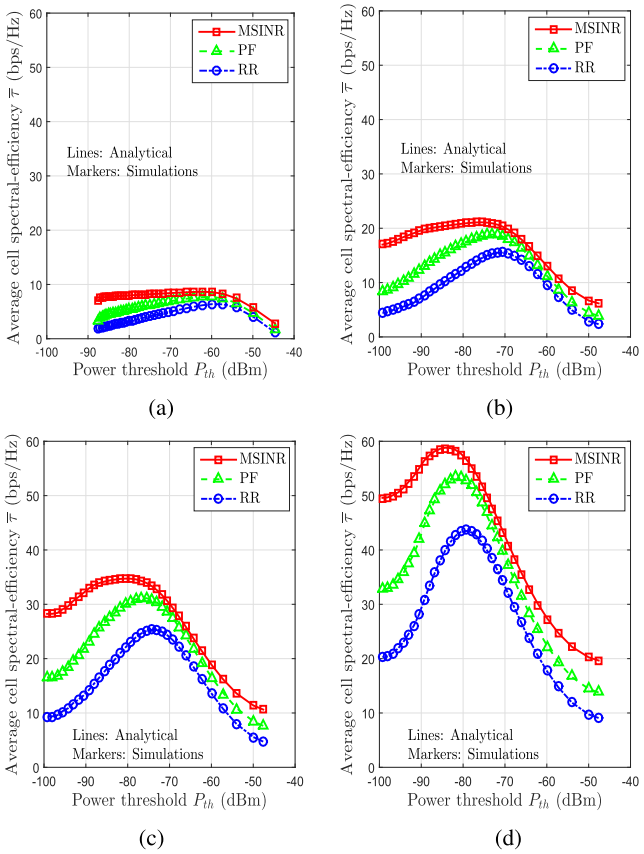

FIGURE 4. Average cell SE versus power threshold P_{th} for omnidirectional and different sectorization deployments, $\Delta = 3$. (a) Omnidirectional. (b) 3 Sectors. (c) 6 Sectors. (d) 12 Sectors.

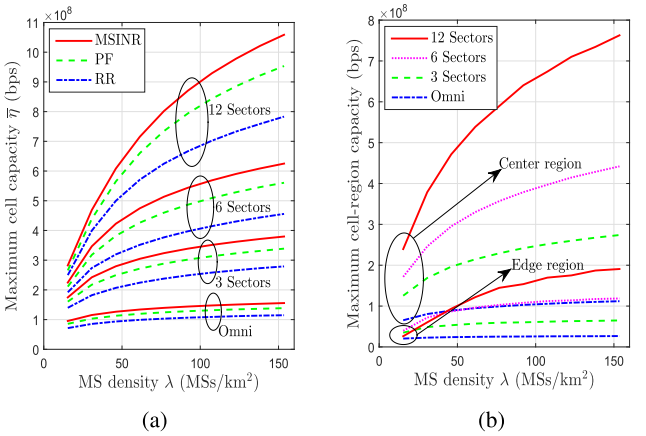

FIGURE 5. Maximum average cell capacity and region capacities versus normalized intensity λ using the optimal P_{th}^{*} value. (a) Maximum $\overline{\eta}$. (b) $N_C\overline{\eta}^C$ and $N_E\overline{\eta}^E$ (PF).

and analyzed when implementing HOS configurations. In this arrangement, shown in Fig. 3, the main directions of the sector antennas are set as in the 3-sector layout case. As in [5] and [33], the spectrum allocation factor ρ used in the scenarios evaluated in this section is set to 0.52 (i.e., MSs located in the center region benefit from 52% of the data bandwidth).

Figure 4 presents the average cell SE as a function of the power threshold P_{th} for $\lambda = 153.5$ MSs/km^2 and under different scheduling policies. Analytical and simulation results are provided for omnidirectional (Fig. 4a), 3 sectors/site (Fig. 4b) and 6 sectors/site (Fig. 4c) deployments. Lines are used to represent analytical results and markers correspond to results obtained through Monte-Carlo simulations. Note the good agreement between the simulated and analytical results, thus validating the analytical framework developed in Sections III and IV. Regarding performance, it can be observed that, as expected, increasing the sectorization order leads to an increase in overall SE. This is basically because the higher the sectorization is, the higher the reutilization of the existing spectrum in the network becomes. For specific cases of channel-aware scheduling techniques (i.e, PF and MSINR) this throughput improvement is further accentuated by the exploitation of the multiuser diversity in comparison to RR. Remarkably, there is an optimal operating point of the FFR power threshold P_{th}^{*} whose value differs for each scheduler in use, and for each sectorization case, hence highlighting the importance of having analytical tools that allow a fast and accurate performance characterization. Note how, irrespective of the scheduler, increasing the sectorization order results in a decrease of the values for the optimal power threshold. This effect is basically due to the fact that the increase in the number of sectors/BS produces a decrease in the levels of ICI and, therefore, the users located in the cell-edge experience higher SINR values. Therefore, the system can increase the SE by reducing the area of the cell-edge regions and placing more MSs in the cell-center.

The optimal P_{th}^{*} values are used in Fig. 5, representing the maximum average cell capacity (see Fig. 5a) and the maximum cell-edge and cell-center capacities (see Fig. 5b) versus normalized intensity λ. The maximum average cell capacity increases with the average number of MSs per area unit (see Fig. 5a). This is basically due to two distinct effects. The first one, fully exploited by the MSINR scheduler, and to a lesser extent by the PF scheduler, is caused by the larger degree of multiuser diversity provided by the increase of λ. The second effect, affecting all the schedulers, is fueled by the fact that increasing the average number of MSs per area unit increments the probability of having at least one center MS and one edge MS, hence reducing the probability of ending up with empty regions, and consequently, unassigned RBs. Figure 5b, assuming the use of a PF scheduler, shows the maximum average capacity for both cell-edge and cell-center regions as a function of the normalized intensity λ (measured in MSs/km^2). Obviously, MSs located in the center region show a better performance. Note that, for HOS deployments, the average edge region capacity decreases for lower MS density values. This is due to the fact that sectors have a smaller angular coverage region for HOS, and the probability that there are sectors without any MS to serve is higher and therefore resources assigned to those empty sectors are wasted. Nevertheless, for higher MS density values, as it is observed in both Fig. 5a and Fig. 5b, increasing the number

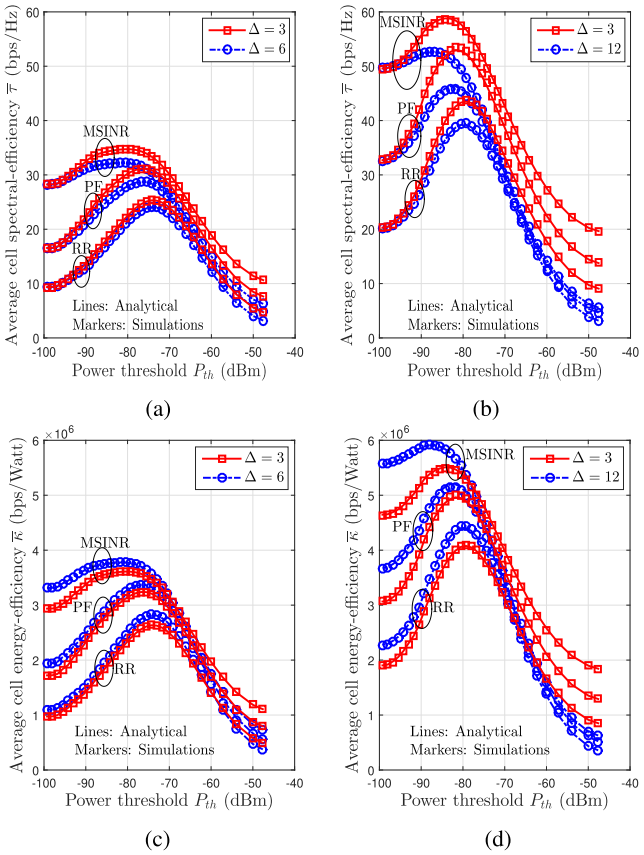

FIGURE 6. Average cell SE and cell EE versus power threshold P_{th} using different cell-edge frequency reuse factor Δ values. (a) SE, 6 Sectors. (b) SE, 12 Sectors. (c) EE, 6 Sectors. (d) EE, 12 Sectors.

of sectors significantly improves the system throughput, as increasing the sectorization order decreases the levels of ICI.

Figure 6 illustrates the impact of the cell-edge frequency reuse factor Δ on both the SE and the EE for a MS density $\lambda = 153.5$ MSs/km^2 and under different scheduling policies. As in Fig. 4, an accurate match is observed between analytical and system level simulation results. By increasing Δ from 3 to N_{sect}, both the average cell capacity and SE decrease due to the reduction of RBs allocated to the edge region (see Figs. 6a and 6b for $N_{\text{sect}} = 6$ and $N_{\text{sect}} = 12$, respectively). However, as it can be observed in Figs. 6c and 6d for $N_{\text{sect}} = 6$ and $N_{\text{sect}} = 12$, respectively, the EE increases when going from $\Delta = 3$ to $\Delta = N_{\text{sect}}$ for lower values of the power threshold (including the optimal P_{th} value). This is due to two distinct effects. First, even though increasing the value of Δ reduces the number of spectral resources available in each sector, it also reduces the number of interfering sectors and, consequently, the levels of ICI experienced by the MSs located at cell-edge. The second effect is caused by the reduction in average power consumption produced by the decrease in the resource utilization coefficient a (see (32)). Notably, although these combined effects do not translate into an SE improvement, they clearly produce an increase of the average EE. That is, even though the spectral partition $\Delta = 3$ seems

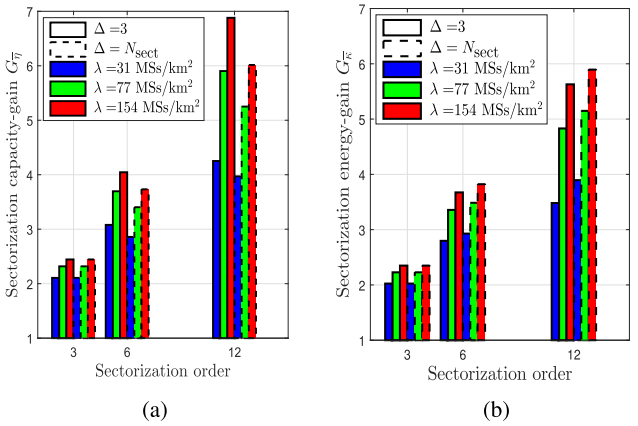

FIGURE 7. Sectorization capacity- and energy-gains versus sectorization order for different normalized intensities (PF). (a) Capacity gain. (b) Energy gain.

to be optimal in terms of the SE metric, using an spectral partition $\Delta = N_{sect}$ is beneficial in terms of the average EE. Hence, choosing a specific setting for Δ will depend on the required tradeoff between SE and EE.

When comparing the average EE for a given Δ value and under different sectorization deployments, it can be observed that the power consumption increases with the number of sectors per site and the average cell capacity. Note however, from Figs. 6c and 6d, that the average EE increases because, even though the power consumption increases with N_{sect}, the average cell capacity increases to a greater extent and fully compensates the increase in energy consumption.

Figure 7 illustrates both the sectorization capacity-gain and the sectorization energy-gain as a function of the sectorization order. Results in these graphs have been obtained assuming the use of the optimal power thresholds P^*_{th}, using the PF scheduling rule and considering different λ values. The bars bordered by continuous lines represent results obtained using $\Delta = 3$, while the bars bordered by dashed lines have been obtained using $\Delta = N_{\text{sect}}$. As in the previous results, it can be observed that both the sectorization capacity-gain and the sectorization energy-gain increase with the sectorization order. In the sectorization capacity-gain case (Fig. 7a), it is important to note that doubling the number of sectors per site (e.g., from 3 to 6, or from 6 to 12) does not produce a doubling of the average cell capacity. Indeed, the capacity-gain is much less than the number of sectors per site. Regarding the cell-edge frequency reuse factor Δ, as in previous figures, the capacity-gain decreases when Δ increases. Considering Fig. 7b, the sectorization energy-gain increases with Δ, due to the decrease in the average power consumption for hight Δ values. This is more noticeable as the sectorization order increases. Indeed, when using $\Delta = 3$, the sectorization energy-gains are much lower that the sectorization capacity-gains. In contrast, sectorization energy-gains are very close to sectorization capacity-gains when using a cell-edge frequency reuse factor $\Delta = N_{\text{sect}}$. Considering the impact of the number of MSs per area unit, it can be observed that both energy- and capacity-gains increase with λ and this can

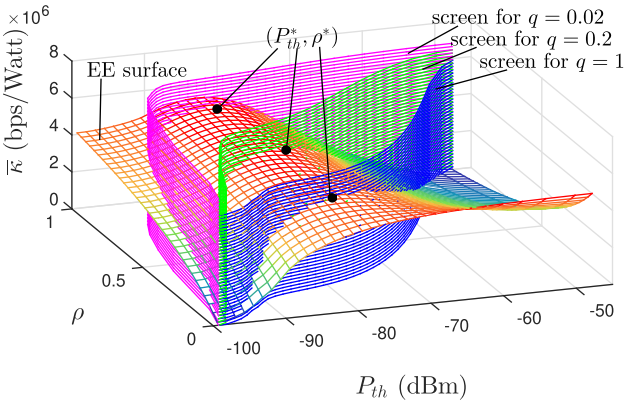

(a)

FIGURE 8. Average cell EE as a function of both the power threshold P_{th} and the spectrum allocation factor ρ (PF). (a) PF scheduler.

basically be attributed to a greater exploitation of the multi-user diversity provided by the use of a PF scheduling rule.

B. EE OPTIMIZATION FOR A 12-SECTOR/BS USE CASE

In this section, optimization problem (36) is solved for a 12-sector/BS deployment targeting the FFR-based optimal parameters (P^*_{th}, ρ^*). Without loss of generality, a cell-edge frequency reuse factor $\Delta = 3$ is used and the main directions of the sector antennas are offset to avoid neighboring sectors pointing at each other (see Fig. 1).

A three-dimensional plot of the average cell EE is shown in Fig. 8 as a function of both P_{th} and ρ when using PF. The EE surface is cut by three "screens" (i.e., three vertical surfaces). Each *screen* is a representation of the function $\rho^\dagger(P_{th})$ along the z-axis for three different quality factors, namely $q = 0.02$, $q = 0.2$ and $q = 1$, corresponding to low, middle and high throughput fairness requirements between cell-center and cell-edge MSs, respectively. The set of operating points provided by the intersection of the EE surface with a given *screen* are those complying with the constraint in (36) for a specific QoS requirement q. Moreover, the operating point in this set (for a specific value of q) leading to the highest average EE is the optimal operating point solving the optimization problem posed in (36). Note that these optimal points, indexed with the label (P^*_{th}, ρ^*), represent the configurations providing maximum average cell EE while satisfying the QoS requirement in (36), for different values of the QoS parameter q. As expected, increasing the QoS requirement q enforces a higher degree of fairness among cell-center and cell-edge MSs at the cost of a decreased average cell EE.

The set of operating points provided by the intersection of the EE surface with the *screens* for $q = 0.02, 0.2$ and 1 are represented using two-dimensional plots in Fig. 9. Fig. 9a shows the average cell EE as a function of P_{th} assuming the use of $\rho^\dagger(P_{th})$. The pairs (P^*_{th}, ρ^*) leading to the maximum average cell EE observed in these graphs are indeed the solutions to problem (36). Note how increasing the QoS requirement q results in higher values for the optimal power threshold P^*_{th} and, consequently, in larger cell-edge regions. Thus, fairness

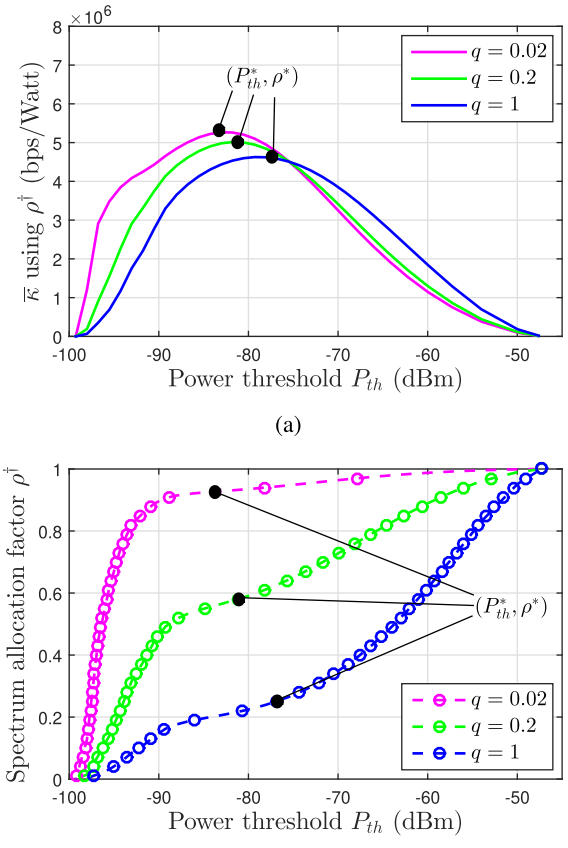

(a)

(b)

FIGURE 9. Average cell EE (using $\rho^\dagger$ values) and $\rho^\dagger$ as functions of the power threshold P_{th} (PF). (a) $\overline{\kappa}(P_{th}, \rho^\dagger)$, PF scheduler. (b) $\rho^\dagger(P_{th})$, PF scheduler.

among MSs is obtained at the cost of sacrificing average cell SE. Figure 9b shows the value of ρ that, for each value of P_{th} and q, fulfills the constraint in (36). The optimal spectrum allocation factor ρ^* decreases when increasing the QoS requirement q. That is, the higher the QoS requirement, the more spectral resources are allocated to the cell-edge users in order to increase the degree of fairness among MSs located in different cell regions.

VI. CONCLUSION

This paper has introduced a novel analytical framework targeting the characterization and performance evaluation of FFR-based OFDMA multi-cellular networks relying on the use of HOS and using channel-aware scheduling techniques. Two fundamentals metrics in the context of 5G networks have been considered, namely, the average cell spectral efficiency and the average energy efficiency. For both metrics, the role played by the sectorization mechanism has been assessed in detail. Results have revealed the synergies created when combining FFR techniques with the use of HOS: while sectorization is capable of increasing both SE and EE specially when using channel-aware scheduling rules able to exploit the multiuser diversity, the FFR component allows the edge users to be adequately served. The cell-edge frequency reuse

factor has been found to impact performance in an antithetical manner: whereas EE improves with an increasing cell-edge frequency reuse factor, the SE decreases, thus making the choice of this parameter dependent of what metric the network designer weighs most. As a method to guarantee a certain degree of cell-edge user performance, a design has been proposed, termed QoScD, that optimizes the FFR related parameters when maximizing the average EE subject to a constraint on the performance achieved by cell-edge users with respect to the central ones. Further work will explore different avenues. Firstly, the framework will be extended so that it can encompass heterogeneous OFDMA-based networks. Secondly, the consideration of shadowing and/or irregular BS deployment will be tackled. Finally, the adaptation of the framework to a massive MIMO setup operating at mmWave frequency will be pursued.

REFERENCES

[1] E. Dahlman, S. Parkvall, and J. Skold, *4G, LTE-Advanced Pro and The Road to 5G*, 3rd ed. New York, NY, USA: Academic, 2016.

[2] C.-X. Wang *et al.*, "Cellular architecture and key technologies for 5G wireless communication networks," *IEEE Commun. Mag.*, vol. 52, no. 2, pp. 122–130, Feb. 2014.

[3] R. Joyce, D. Morris, S. Brown, D. Vyas, and L. Zhang, "Higher order horizontal sectorization gains for 6, 9, 12 and 15 sectored cell sites in a 3GPP/HSPA+ network," *IEEE Trans. Veh. Technol.*, vol. 65, no. 5, pp. 3440–3449, May 2016.

[4] L. H. Nguyen and A. Weber, "Higher order sectorization in LTE downlink with 3GPP release 10 closed loop MIMO transmission techniques," in *Proc. 20th Int. ITG Workshop Smart Antennas (WSA)*, Mar. 2016, pp. 1–8.

[5] J. He, W. Cheng, Z. Tang, D. López-Pérez, and H. Claussen, "Analytical evaluation of higher order sectorization, frequency reuse, and user classification methods in OFDMA networks," *IEEE Trans. Wireless Commun.*, vol. 15, no. 12, pp. 8209–8222, Dec. 2016.

[6] A. Arbi and T. O'Farrell, "Energy efficiency in 5G access networks: Small cell densification and high order sectorisation," in *Proc. IEEE Int. Conf. Commun. Workshop (ICCW)*, Jun. 2015, pp. 2806–2811.

[7] E. Dahlman, S. Parkvall, and J. Sköld, *4G: LTE/LTE-Advanced for Mobile Broadband*, 2nd ed. Amsterdam, The Netherlands: Elsevier, 2013.

[8] A. S. Hamza, S. S. Khalifa, H. S. Hamza, and K. Elsayed, "A survey on inter-cell interference coordination techniques in OFDMA-based cellular networks," *IEEE Commun. Surveys Tuts.*, vol. 15, no. 4, pp. 1642–1670, 4th Quart., 2013.

[9] X. Yang, "A multilevel soft frequency reuse technique for wireless communication systems," *IEEE Commun. Lett.*, vol. 18, no. 11, pp. 1983–1986, Nov. 2014.

[10] H. Lei, L. Zhang, X. Zhang, and D. Yang, "A novel multi-cell OFDMA system structure using fractional frequency reuse," in *Proc. IEEE 18th Int. Symp. Pers., Indoor Mobile Radio Commun. (PIMRC)*, Sep. 2007, pp. 1–5.

[11] J. García-Morales, G. Femenias, and F. Riera-Palou, "Statistical analysis and optimization of a fifth-percentile user rate constrained design for FFR/SFR-aided OFDMA-based cellular networks," *IEEE Trans. Veh. Technol.*, vol. 67, no. 4, pp. 3406–3419, Apr. 2018.

[12] G. Femenias and F. Riera-Palou, "Corrections to and comments on 'throughput and optimal threshold for FFR schemes in OFDMA cellular networks,'" *IEEE Trans. Wireless Commun.*, vol. 14, no. 5, pp. 2926–2928, May 2015.

[13] J. García-Morales, G. Femenias, F. Riera-Palou, and J. S. Thompson, "Multi-layer FFR-aided OFDMA-based networks using channel-aware schedulers," *IEEE Access*, vol. 6, pp. 7134–7147, 2018.

[14] R. Knopp and P. A. Humblet, "Information capacity and power control in single-cell multiuser communications," in *Proc. IEEE Int. Conf. Commun.*, vol. 1, Jun. 1995, pp. 331–335.

[15] F. P. Kelly, A. K. Maulloo, and D. K. H. Tan, "Rate control for communication networks: Shadow prices, proportional fairness and stability," *J. Oper. Res. Soc.*, vol. 49, no. 3, pp. 237–252, Mar. 1998.

[16] S. Shakkottai and A. L. Stolyar, "Scheduling algorithms for a mixture of real-time and non-real-time data in HDR," in *Teletraffic Engineering in the Internet Era* (Teletraffic Science and Engineering), vol. 4, J. M. de Souza, N. L. S. da Fonseca, and E. A. de Souza e Silva. Amsterdam, The Netherlands: Elsevier, 2001, pp. 793–804. [Online]. Available: http://www.sciencedirect.com/science/article/pii/S1388343701801700, doi: 10.1016/S1388-3437(01)80170-0.

[17] J. García-Morales, G. Femenias, and F. Riera-Palou, "Analysis and optimization of FFR-aided OFDMA-based heterogeneous cellular networks," *IEEE Access*, vol. 4, pp. 5111–5127, 2016.

[18] H. Huang *et al.*, "Increasing throughput in cellular networks with higher-order sectorization," in *Proc. Conf. Rec. 44th Asilomar Conf. Signals, Syst. Comput. (ASILOMAR)*, Nov. 2010, pp. 630–635.

[19] M. U. Sheikh and J. Lempiäinen, "Migration to 28 GHz frequency with higher order sectorization in urban macro cellular environment," in *Proc. 23rd Int. Conf. Telecommun. (ICT)*, May 2016, pp. 1–5.

[20] N. Al-Falahy and O. Y. K. Alani, "The impact of higher order sectorisation on the performance of millimetre wave 5G network," in *Proc. 10th Int. Conf. Next Gener. Mobile Appl., Secur. Technol. (NGMAST)*, Aug. 2016, pp. 1–5.

[21] L. A. Ferhi, K. Sethom, and F. Choubani, "Multi-carrier 3D beamforming for 5G ultra-dense cellular networks," in *Proc. Int. Conf. Adv. Syst. Electr. Technol. (ICASET)*, Mar. 2018, pp. 221–226.

[22] N. Al-Falahy and O. Y. K. Alani, "Network capacity optimisation in millimetre wave band using fractional frequency reuse," *IEEE Access*, vol. 6, pp. 10924–10932, 2018.

[23] M. Agiwal, A. Roy, and N. Saxena, "Next generation 5G wireless networks: A comprehensive survey," *IEEE Commun. Surveys Tuts.*, vol. 18, no. 3, pp. 1617–1655, 3rd Quart., 2016.

[24] B. Xie, Z. Zhang, R. Q. Hu, G. Wu, and A. Papathanassiou, "Joint spectral efficiency and energy efficiency in FFR-based wireless heterogeneous networks," *IEEE Trans. Veh. Technol.*, vol. 67, no. 9, pp. 8154–8168, Sep. 2018.

[25] Y. Xu, X. Xu, Y. Li, X. Chen, and X. Tao, "Energy-efficient power control for fractional frequency reuse," in *Proc. IEEE 24th Annu. Int. Symp. Pers., Indoor, Mobile Radio Commun. (PIMRC)*, Sep. 2013, pp. 2962–2966.

[26] C. Altay and M. Koca, "Capacity analysis and optimization of fractional frequency reuse under energy efficiency constraints," in *Proc. IEEE Wireless Commun. Netw. Conf. (WCNC)*, Apr. 2018, pp. 1–6.

[27] S. Tombaz, A. Vastberg, and J. Zander, "Energy- and cost-efficient ultra-high-capacity wireless access," *IEEE Wireless Commun.*, vol. 18, no. 5, pp. 18–24, Oct. 2011.

[28] E. Björnson, L. Sanguinetti, J. Hoydis, and M. Debbah, "Optimal design of energy-efficient multi-user MIMO systems: Is massive MIMO the answer?" *IEEE Trans. Wireless Commun.*, vol. 14, no. 6, pp. 3059–3075, Jun. 2015.

[29] J. García-Morales, G. Femenias, and F. Riera-Palou, "FFR-aided OFDMA-based networks under spatially correlated shadowing," in *Proc. IEEE 13th Int. Conf. Wireless Mobile Comput., Netw. Commun. (WiMob)*, Oct. 2017, pp. 49–54.

[30] D. González, M. García-Lozano, S. Ruiz, M. A. Lema, and D. Lee, "Multiobjective optimization of fractional frequency reuse for irregular OFDMA macrocellular deployments," *Telecommun. Syst.*, vol. 61, no. 4, pp. 659–673, 2016.

[31] T. Novlan, R. Ganti, A. Ghosh, and J. Andrews, "Analytical evaluation of fractional frequency reuse for OFDMA cellular networks," *IEEE Trans. Wireless Commun.*, vol. 10, no. 12, pp. 4294–4305, Dec. 2011.

[32] F. Jin, R. Zhang, and L. Hanzo, "Fractional frequency reuse aided twin-layer femtocell networks: Analysis, design and optimization," *IEEE Trans. Commun.*, vol. 61, no. 5, pp. 2074–2085, May 2013.

[33] Z. Xu, G. Y. Li, C. Yang, and X. Zhu, "Throughput and optimal threshold for FFR schemes in OFDMA cellular networks," *IEEE Trans. Wireless Commun.*, vol. 11, no. 8, pp. 2776–2785, Aug. 2012.

[34] J. García-Morales, G. Femenias, and F. Riera-Palou, "On the design of OFDMA-based FFR-aided irregular cellular networks with shadowing," *IEEE Access*, vol. 6, pp. 7641–7653, 2018.

[35] J. García-Morales, G. Femenias, and F. Riera-Palou, "On the analysis of channel-aware schedulers in OFDMA-based networks using FFR," in *Proc. 11th Int. Conf. Wireless Mobile Comput., Netw. Commun. (WiMob)*, Oct. 2015, pp. 786–793.

[36] R. V. R. Kumar and J. Gurugubelli, "How green the LTE technology can be?" in *Proc. 2nd Int. Conf. Wireless Commun., Veh. Technol., Inf. Theory Aerosp. Electron. Syst. Technol. (Wireless VITAE)*, Feb./Mar. 2011, pp. 1–5.

[37] H. Q. Ngo, L.-N. Tran, T. Q. Duong, M. Matthaiou, and E. G. Larsson, "On the total energy efficiency of cell-free massive MIMO," *IEEE Trans. Green Commun. Netw.*, vol. 2, no. 1, pp. 25–39, Mar. 2018.
[38] J. Tang, D. K. C. So, E. Alsusa, and K. A. Hamdi, "Resource efficiency: A new paradigm on energy efficiency and spectral efficiency tradeoff," *IEEE Trans. Wireless Commun.*, vol. 13, no. 8, pp. 4656–4669, Aug. 2014.
[39] J. García-Morales, G. Femenias, and F. Riera-Palou, "Statistical analysis and optimization of FFR/SFR-aided OFDMA-based multi-cellular networks," in *Proc. IEEE Stat. Signal Process. Workshop (SSP)*, Jun. 2016, pp. 1–5.
[40] *Home Enode B (HeNB) Radio Frequency (RF) Requirements Analysis (Release 9) v9.0.0.*, document G. TR36.921, 2010.

JAN GARCÍA-MORALES (S'14) was born in Cienfuegos, Cuba, in 1984. He received the degree in telecommunications and electronics from the Faculty of Electrical Engineering, Central University of Las Villas, Villa Clara, Cuba, in 2008, the M.Sc. degree in information technologies from the Department of Mathematics and Informatics, University of the Balearic Islands (UIB), in 2013, and the Ph.D. degree in the Information and Communication Technologies Program from UIB, in 2018. He was with Innovation and Technology Company IBITEC S.L., as a Santander-Crue-Cepyme Internship Researcher Assistant, conducting research on designing and programming automatic systems and sensor networks. He was with Mobile Telecommunications Company MOVITEL S.A., from 2008 to 2012. Motivated by the research in the telecommunications and information technology area, he applied for one of the Santander-Iberoamerica Scholarship, in 2012, to enroll in the master's degree (research itinerary) in Spain. From 2013 to 2018, he was a member of the Mobile Communications Group, UIB. Since 2018, he has been a Post-Doctoral Researcher with the UWICORE Laboratory, Universidad Miguel Hernández de Elche, Spain. In 2013, he received a Pre-Doctoral Scholarship from the Conselleria d'Educació, Cultura i Universitats, Govern de les Illes Balears, under Grant FPI/1538/2013, as part of an operational program co-financed by the European Social Fund.

GUILLEM FEMENIAS (SM'11) received the degree in telecommunication engineering and the Ph.D. degree in electrical engineering from the Technical University of Catalonia (UPC), Barcelona, Spain, in 1987 and 1991, respectively. From 1987 to 1994, he was a Researcher with UPC, where he became an Associate Professor, in 1992. In 1995, he joined the Department of Mathematics and Informatics, University of the Balearic Islands (UIB), Mallorca, Spain, where he became a Full Professor, in 2010. He is currently leading the Mobile Communications Group, UIB, where he has been the Project Manager of projects ARAMIS, DREAMS, DARWIN, MARIMBA, COSMOS, ELISA, and TERESA, all of them funded by the Spanish and Balearic Islands Governments. In the past, he was also involved with several European projects (ATDMA, CODIT, and COST). His current research interests and activities span the fields of digital communications theory and wireless communication systems, with a particular emphasis on cross-layer transceiver design, resource management, and scheduling strategies applied to fourth- and fifth-generation wireless networks. On these topics, he has published more than 90 journal and conference papers, and some book chapters. He was a recipient of the Best Paper Awards at the 2007 IFIP International Conference on Personal Wireless Communications and the 2009 IEEE Vehicular Technology Conference (VTC-Spring 2009). He has served for various IEEE conferences as a Technical Program Committee Member, as the Publications Chair for the IEEE 69th VTC-Spring 2009, and as the Local Organizing Committee Member of the IEEE Statistical Signal Processing (SSP 2016).

FELIP RIERA-PALOU (SM'11) received the B.S./M.S. degree in computer engineering from the University of the Balearic Islands (UIB), Mallorca, Spain, in 1997, the M.Sc. and Ph.D. degrees in communication engineering from the University of Bradford, U.K., in 1998 and 2002, respectively, and the M.Sc. degree in statistics from The University of Sheffield, U.K., in 2006. From 2002 to 2005, he was with Philips Research Laboratories, Eindhoven, The Netherlands, first as a Marie Curie Postdoctoral Fellow (European Union) and later as a Member of Technical Staff. While at Philips, he was involved in research programs related to wideband speech/audio compression and speech enhancement for mobile telephony. From 2005 to 2009, he was a Research Associate (Ramon y Cajal Program, Spanish Ministry of Science) with the Mobile Communications Group, Department of Mathematics and Informatics, UIB, where he has been an Associate Research Professor (I3 Program, Spanish Ministry of Education), since 2010. His current research interests include signal processing and wireless communications.